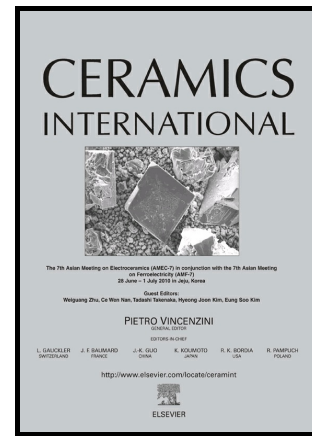


# Author's Accepted Manuscript

## Impact of Microwave Processing on Porcelain Microstructure

Wirat Lerdprom, Eugenio Zapata-Solvas, Doni. D. Jayaseelan, Amparo Borrell, Maria. D. Salvador, William. E. Lee



[www.elsevier.com/locate/ceri](http://www.elsevier.com/locate/ceri)

PII: S0272-8842(17)31520-1  
DOI: <http://dx.doi.org/10.1016/j.ceramint.2017.07.090>  
Reference: CER115810

To appear in: *Ceramics International*

Received date: 2 December 2016  
Revised date: 27 April 2017  
Accepted date: 11 July 2017

Cite this article as: Wirat Lerdprom, Eugenio Zapata-Solvas, Doni. D. Jayaseelan, Amparo Borrell, Maria. D. Salvador and William. E. Lee, Impact of Microwave Processing on Porcelain Microstructure, *Ceramics International*, <http://dx.doi.org/10.1016/j.ceramint.2017.07.090>

This is a PDF file of an unedited manuscript that has been accepted for publication. As a service to our customers we are providing this early version of the manuscript. The manuscript will undergo copyediting, typesetting, and a review of the resulting galley proof before it is published in its final citable form. Please note that during the production process errors may be discovered which could affect the content, and all legal disclaimers that apply to the journal pertain.

# Impact of Microwave Processing on Porcelain Microstructure

Wirat Lerdprom<sup>1</sup>, Eugenio Zapata-Solvas<sup>1</sup>, Doni. D. Jayaseelan<sup>2</sup>, Amparo Borrell<sup>3</sup>,  
Maria. D. Salvador<sup>3</sup> William. E. Lee<sup>1</sup>

<sup>1</sup>Centre for Advanced Structural Ceramics, Department of Materials, Imperial College London, South Kensington Campus, London, SW7 2AZ, UK

<sup>2</sup>School of Mechanical and Aerospace Engineering, Faculty of Science, Engineering and Computing, Kingston University London, Roehampton Vale Campus, London, SW15 3DW, UK

<sup>3</sup>Instituto de Tecnología de Materiales (ITM), Universitat Politècnica de València, Camino de Vera, s/n, 46022 Valencia, Spain

## Abstract

Microstructural evolution on sintering of porcelain powder compacts using microwave radiation was compared with that in conventionally sintered samples. Using microwaves sintering temperature was reduced by ~ 75 °C and dwell time from 15 min to 5 min while retaining comparable physical properties i.e. apparent bulk density, water absorption to conventionally sintered porcelain. Porcelain powder absorbed microwave energy above 600 °C due to a rapid increase in its loss tangent. Mullite and glass were used as indicators of the microwave effect: mullite produced using microwaves had a nanofibre morphology with high aspect ratio (~32±3:1) believed associated with a vapour-liquid-solid (VLS) formation mechanism not previously reported. Microwaves also produced mullite with different chemistry having ~63 mol% alumina content compared to ~60 mol% alumina in conventional sintered porcelain. This was likely due to accelerated Al<sup>3+</sup> diffusion in mullite under microwave radiation. Liquid glass was observed to form at relatively low temperature (~900-1000°C) using microwaves when compared to conventional sintering which promoted the porcelains ability to absorb them.

**Keywords:** Porcelain, Aluminosilicate, Mullite, Microwave sintering, Field assisted sintering technique

## I. Introduction

Use of microwaves for material processing has accelerated in recent years because they provide a promising alternative energy source potentially reducing total energy consumption<sup>[1-3]</sup>. Microwaves are absorbed directly in bulk materials allowing volumetric heating and inducing enhanced diffusion rates<sup>[2]</sup>. The materials are heated via dipole rotation under microwave field and lose their energy by collisions. Microwave sintering is also a selective heating process so that almost all microwaves are converted to energy. Since it is volumetric heating, the temperature profile in the sample bulk is inverse due to thermal heat loss at the sample surface (inside is hotter than surface); thus, a potential drawback of microwave heating, in samples with low thermal conductivity, is the 'thermal runaway effect' (an uncontrolled temperature rise inside the sample). Thermal runaway may lead to a non-uniform microstructure or localized melting<sup>[4, 5]</sup> but it can be mitigated by using the microwave heating associating with conventional firing process so called hybrid microwave heating minimizing temperature gradient throughout a sample<sup>[6, 7]</sup>.

The successful application of microwave sintering depends on the dielectric properties of the materials—mainly dielectric constant, dielectric loss, loss tangent and penetration depth—at a certain microwave frequency (2.45 GHz is typically used for materials processing). The dielectric constant ( $\epsilon'$ ) defines the ability of ions and dipole to reorient under an alternating electric field while dielectric loss ( $\epsilon''$ ) represents heat generation during material coupling with the alternating electric field. Both values are used to calculate loss tangent ( $\tan \delta$ ) representing how much heat is generated in materials. The penetration depth ( $D_p$ ) is defined as the distance which the intensity of the applied electromagnetic fields decays to  $1/e$ . Generally, loss tangent ranging from 0.01-1 are suitable for microwave processing<sup>[8]</sup>. Furthermore, dielectric properties of most materials are temperature dependent resulting in more microwave energy is absorbed at elevated temperature. These changes of dielectric properties may also lead to thermal runaway.

Porcelains and their raw materials are poorly microwave absorbing materials, all of which do not couple well with microwaves at room temperature but they can

effectively absorb microwaves above a critical temperature<sup>[9, 10]</sup> Thus, it is possible to process porcelains using microwaves at elevated temperature. Generally, porcelains are vitreous ceramics derived from triaxial mixtures of clay minerals, feldspars, and quartz. After heat treatment, fired porcelains comprise of mullite, glass and residual quartz<sup>[11-13]</sup>. Several chemical reactions occur during firing of porcelains including dehydroxylation of the clays from ~ 450-600 °C, glass formation by feldspar melting at ~990-1050 °C (depending on its chemistry), and partial quartz dissolution >1200 °C<sup>[11, 13]</sup>. Mullite starts to form around 940-980 °C and different types of mullite are observed depending on sources. Primary mullite forms by the clay decomposition and found in the clay relicts while secondary mullite forms from the reaction of the clay and feldspar melt, and found in the glass region<sup>[12, 14]</sup>. These transformations can also change the dielectric properties of the porcelain being fired affecting its microwave absorbability.

Uses of microwave energy to sinter porcelains have been reported. *Menezes et al.*<sup>[15]</sup> successfully produced different porcelain bodies including sanitaryware, dental and electrical porcelains using a 2.45 GHz hybrid microwave sintering system (infrared heat and a susceptor were used). Water absorption was at the same level as in conventionally sintered porcelain, but the maturing temperature of microwave sintering was higher ~20 °C compared with the conventional one. However, substantial reduction of dwell time was observed with microwave sintering. Microwave sintering of high voltage porcelain insulators found better properties (density, modulus of rupture, and dielectric strength) compared to conventional sintered at the same maturing temperature, and the firing time was reduced ~80%<sup>[16]</sup>.

*Shawn et al.*,<sup>[17]</sup> successfully produced a large-cross section (12 cm of diameter) electrical porcelain insulator using Microwave Assisted Technology (MAT), a combination of electric furnace and microwave heating, with 5 times shorter processing time compared to the conventional process.

*Santos et al.*,<sup>[18]</sup> developed a multimode cavity (2.45 GHz) microwave oven which was capable of firing porcelain tableware with a SiC slab as a support. The microwave sintered porcelains showed similar impact resistance, porosity, water absorption, and phase compositions to conventionally sintered porcelains. The microwave sintering process was faster resulting in lower processing costs. An important aspect of their work was the effect of microwave power distribution in the

cavity resulting in homogeneity on the sample. A critical problem in microwave sintering was thermal runaway due to inhomogeneous microwave absorption. To combat this *Monteiro et al.*,<sup>[19]</sup> developed a control system which created a uniform electromagnetic field and therefore more uniform heating, even at high heating rates. Even, there were several studies dealing with the microwave sintering of porcelains but none have reported in detail the effect of microwave heating on microstructural evolution, thus in the present study the effect of microwave radiation on mullite formation, and porcelain densification will be discussed.

Accepted manuscript

## II. Experimental

The raw material used in this work was spray dried porcelain powder provided by a tile manufacturer, used in as-received form without any reprocessing consisting of kaolinite, albite and quartz. The powder was uniaxially cold-pressed using 35 MPa into 13 mm diameter and 7 mm thick pellets in a steel die. The pellets were dried overnight at 110 °C and stored in an oven until further experiments.

Thermal behaviour of the spray dried powder, with mean particle size ( $D_{50}$ ) of 10  $\mu\text{m}$ , was characterised by using a simultaneous thermogravimetry-differential thermal analyzer (TG-DTA, Netzsch STA 449C, Jupiter, Selb, Germany) under continuous air flow at a rate of 50 ml/h from 25-1200 °C at a heating rate of 10 °C/min and instrument cooling rate.

The pellets were sintered under air in a single mode cylindrical microwave cavity operating in the  $TE_{111}$  mode with a resonant frequency of 2.45 GHz<sup>[20]</sup>—a quartz tube was used as sample holder (Fig.1a). The furnace E-field has maximum ( $E_r$  and  $E_\phi$  components) in the center, where the samples are located<sup>[21]</sup>. The final temperatures reached were 850, 900, 1000 and 1100 °C using a heating rate of ~30 °C/min with 5 min of holding time at the respective temperatures. The temperature of the sample was monitored using an infrared radiation thermometer (Optris CT-Laser LT, 8–14  $\mu\text{m}$ ), focused on the sample surface. Since the interior temperature was higher than that in the surface of the samples. Thus, a simple simulation work was performed using a finite element analysis (FEA) software package, COMSOL Multiphysics V. 5.2a to show the temperature profile. Electromagnetic parameter used in the simulation were relative permittivity of the air in the cavity=1.0. Cavity walls was perfectly conducting. Heat transfer parameters were (1) heat capacity= 920(J/kg·K), (2) thermal conductivity = 0.582(W/m·K), (3) electrical conductivity=0.014(S/m), and density= 2.003 (g/cm<sup>3</sup>).

Initially, pellets were exposed to the microwaves with neither insulation nor susceptor used. As a result, they were not sintered uniformly. A small well-sintered region (~5 mm<sup>3</sup>) in the middle of the sample indicated a need to modify the setup as presented in Fig.1b. Finally, silicon carbide powder as susceptor and alumina insulation were used to promote uniform temperature distribution (Fig.1b). For comparison, the same porcelain pellets were conventionally sintered at 850, 900,

1000, 1100, 1175 and 1200 °C using a heating rate of 10 °C/min with 15 min hold at each temperature.

Apparent bulk density (ABD) and water absorption (WA) of dense samples were obtained using an ASTM standard (C20-00) immersion method. The samples were cut prior performing ABD and WA measurements to prevent error from seal surfaces. Phase analyses of the sintered samples were carried out using X-ray diffraction (XRD, Bruker D2 Phaser, Madison, WI, USA). XRD data were collected from 15° to 65° 2 $\theta$  with CuK $\alpha$  radiation ( $\lambda=0.154$  nm) at 30kV and 10 mA with a step size of 0.03° and a count time of 1 s. Diffraction patterns were analyzed using commercial software (X'pert high score plus software, Pan Analytical). Mullite chemistry was calculated from the XRD line broadening using Ban and Okada equation [25]. The sample surfaces were ground and polished using silicon carbide abrasive sheets (800,1200, 2400 and 4000 grits) and the polished surfaces were etched using 5% HF for 15 seconds to reveal their microstructures. Microstructures were examined using a scanning electron microscope, SEM, (Auriga: Carl Zeiss; Oberkochen, Germany) at an accelerating voltage of 5 kV, under high vacuum mode and using secondary electron imaging (SEI).

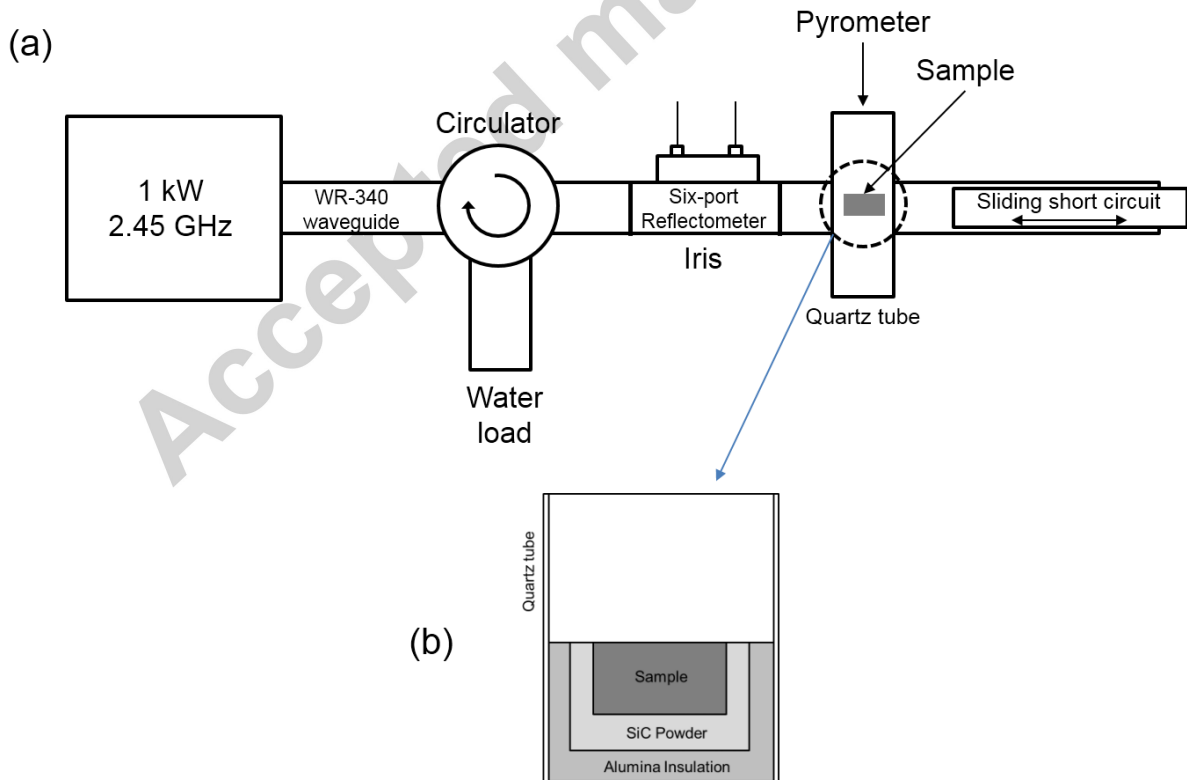


Fig.1. a) schematic view of the microwave sintering cavity, b) the sample environment in the microwave cavity.

Accepted manuscript

### III. Results and discussion

Fig.2 shows development of ABD and WA as a function of sintering temperature for conventionally and microwave sintered samples. Densification of the porcelain using microwave energy started at relatively low temperature ( $\sim 850^\circ\text{C}$ , surface temperature measured using the pyrometer) compared with samples fired in the absence of microwave radiation, which started to densify at  $\sim 1100^\circ\text{C}$ . However, it is noted that inside temperature under microwave irradiation was higher than that at the surface. Thus, a FEA work was performed to estimate the interior temperature. Fig.2 also suggests that the estimated temperature for densification process under microwave sintering was about  $100^\circ\text{C}$  higher than that measured using the pyrometer. Thus, an estimated temperature curve was added to represent inside temperature of the sample sintering under microwave radiation. Therefore, densification of this porcelain under microwave radiation started at  $\sim 950^\circ\text{C}$  and achieved full densification at  $\sim 1100^\circ\text{C}$  which was  $\sim 75^\circ\text{C}$  lower than that in the conventional sintering process.

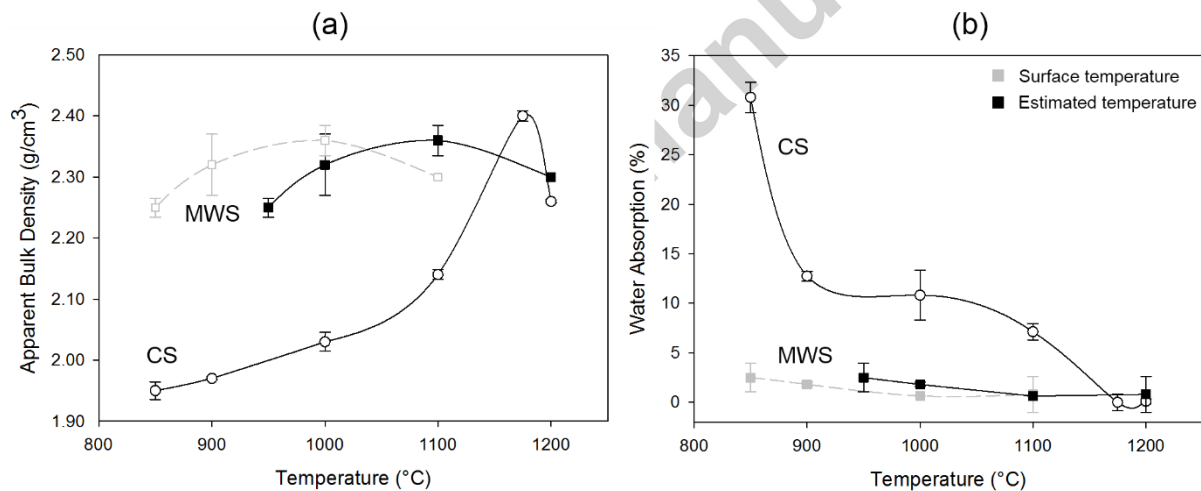


Fig.2. a) ABD and b) WA of conventionally (CS) and microwave sintered (MWS) porcelains as a function of temperature. Note that  $10^\circ\text{C}/\text{min}$  and 15 min dwell were used in CS while  $30^\circ\text{C}/\text{min}$  and 5 min dwell were used in MWS.

Fig.3a reveals the sample's surface temperature of  $850^\circ\text{C}$  monitored using the pyrometer corresponding to  $\sim 1100^\circ\text{C}$  of the inside temperature estimated by FEA. It can be seen that the microstructure in Fig.3a was in good agreement with the simulation work (Fig.3b). The interior temperature (at well sintered region) was about  $100\text{-}250^\circ\text{C}$  higher than that measured at the sample surfaces. This observation also agreed with the microstructure of the sample showing a bisque-characteristic at the

top surface. At the middle of the sample, the estimated temperature was about 1100°C which indicated by the well-sintered microstructure. At the bottom of the sample, large bubbles were observed indicating high temperature (>1175°C, the optimum firing temperature of the sample under a conventional firing process), the FEA result showed temperature as high as 1300°C. It is important to note that porcelains densify via viscous flow mechanism thus, forming large amount of liquid glass phase is the main factor. Since the melting process of feldspars is a thermodynamically limited therefore it is independent on the energy routes introduced to the system. In other words, the densification temperature (melting of feldspars) of the both processes were not much different which is about ~75°C.

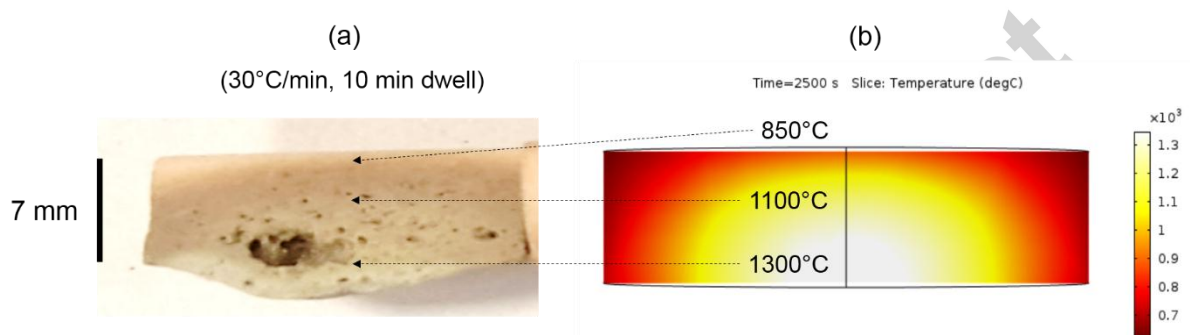


Fig.3. (a) microstructure of the microwave sintered sample using 30°C/min, 10 min dwell at surface temperature of 850°C. (b) FEA result showing the temperature profile which agrees with the actual sample.

Conventionally sintered samples reached their maximum ABD (2.40 g/cm<sup>3</sup>) after firing at 1175 °C whereas the microwave sintered sample reached its maximum ABD (2.36 g/cm<sup>3</sup>) at 1100 °C, beyond these temperatures the ABD decreased. The WA of the samples sintered using microwave was lower than the conventionally sintered samples from 950-1100 °C indicating these samples had better degree of densification, but once the samples reached their maximum ABD, conventionally sintered samples had WA of 0.1% while microwave sintered samples had WA of 0.8%. The difference of maximum ABD and WA resulted from the different microstructure of the samples as shown in Fig.4. Furthermore, increasing WA associated with decreasing ABD was due to a bloating effect which is a common phenomenon when porcelains are fired beyond the optimal temperature [12-14].

Fig.4a compares the thermal profile of the fully sintered samples sintered using conventional (10 °C/min, 1175 °C, 15 min dwell) and microwave (30 °C/min, 1100 °C, 5 min dwell) processes. Excluding the cooling step, the densification was 3

times shorter by microwave processing to produce fully dense sample compared to the CS process. SEI (Fig.4b) reveals distinct microstructures. CS samples were dense with small pores (<30  $\mu\text{m}$  of diameter) were observed in the glass matrix whereas MWS samples contained large pores (>300  $\mu\text{m}$  of diameter) which was due to over firing. The large pores in the MWS samples were formed in liquid glass melt during microwave radiation and those large pores represented an overfiring temperature. It was reasonable that melting of feldspar produced liquid glass changing the sample dielectric properties <sup>[23]</sup>, so that the sample absorbed more microwave energy, thus the temperature rose uncontrollably.

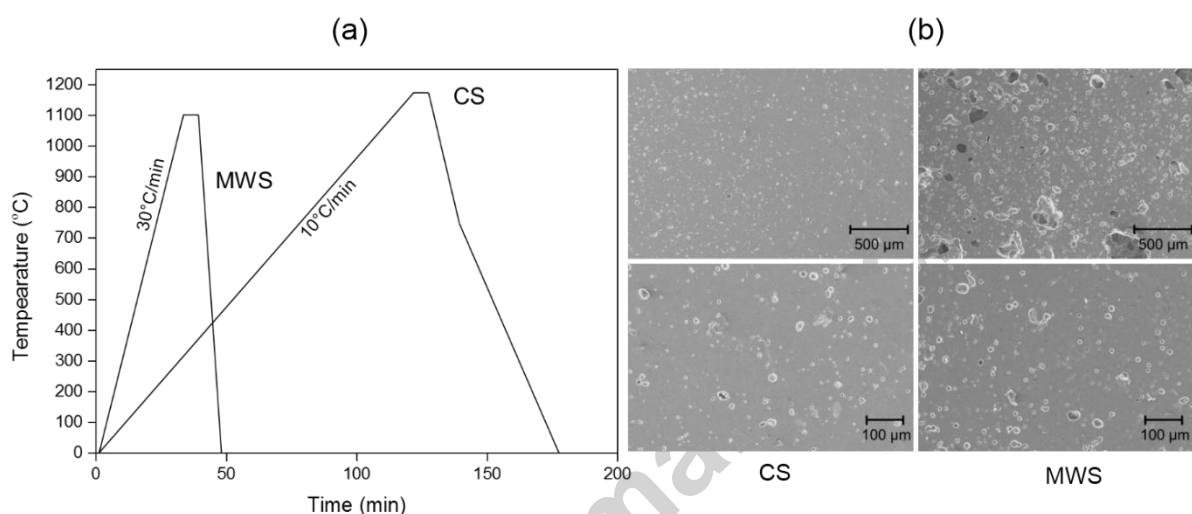


Fig.4. a) Sintering curves of conventional and microwave heat treatments, b) SEM-SEI images of conventionally sintered (CS) and microwave sintered (MWS) porcelain samples.

The thermal behaviour of the green porcelain powder conventionally sintered (Fig.5) reveals total weight loss ~5%, 1% from physically-bound evaporation, and 4% from chemically-bound water decomposition from the clays. The two large endothermic peaks arose from evaporation of physically-bound water at 100-200 °C and dehydroxylation of chemically-bound water of the clay between 450-600 °C. However, the endothermic peak of the  $\alpha$ - $\beta$  quartz inversion at 573 °C was masked by overlap with the clay dehydroxylation peak. The small exothermic peak around ~940 °C suggested initial formation of the spinel-alumina phase from the clay species <sup>[11-14, 28, 29]</sup>. This thermal behaviour implied that changing thermal behaviour of the powder at elevated temperature changed its ability to absorb microwaves. Fig.6 shows dielectric behaviour of the porcelain sample under alternating electric field of 1 MHz. Fig.6a presents the calculated loss tangent of the porcelain powder

from room temperature to 900 °C using  $\tan \delta = \sigma/2\pi f \epsilon_0$ , where  $\sigma$  is overall electrical conductivity,  $f$  is frequency of alternating electric field, and  $\epsilon_0$  is permittivity of free space ( $\epsilon_0 = 8.85 \times 10^{-12} \text{ F}\cdot\text{m}^{-1}$ ). The electrical conductivity of the porcelain sample was obtained elsewhere<sup>[30]</sup>.

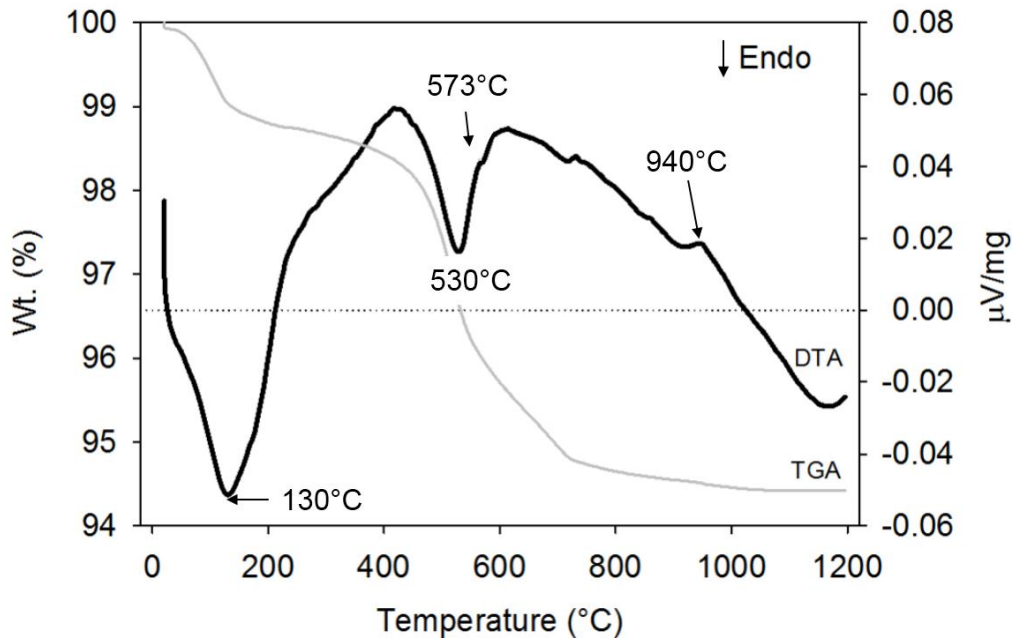


Fig.5. Thermal behaviour (TGA and DTA) of porcelain powder.

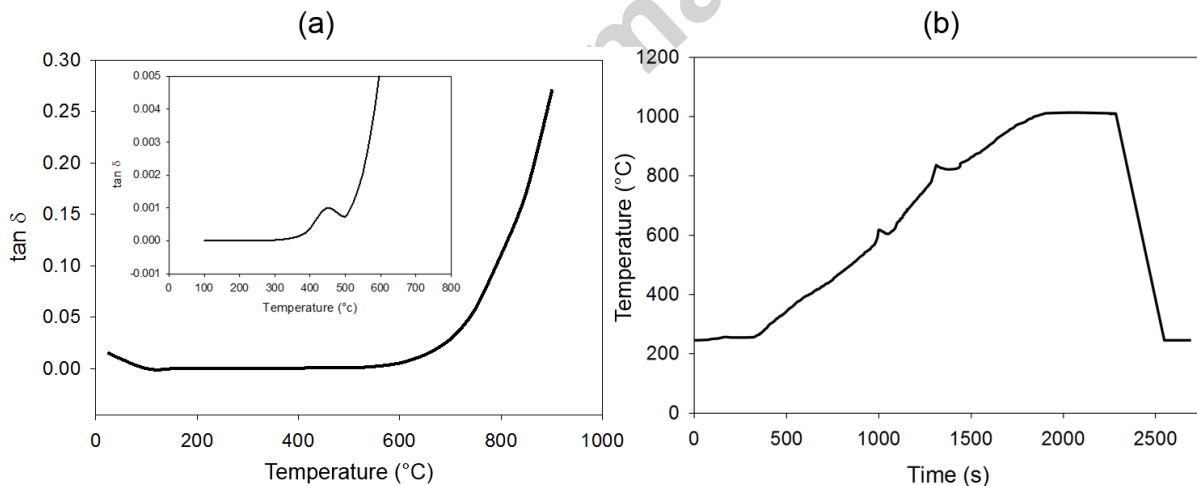


Fig.6. (a) Calculated loss tangent ( $\tan \delta$ ) of the porcelain sample as a function of temperature, the inset shows detail at 400-500°C, and (b) the temperature profile of microwave sintering (1000°C, 30°C/min, 5 min dwell) shows 2 humps at 600 and 800°C (interior temperature) corresponding to the rapid change of the  $\tan \delta$ .

Generally, microwave energy is effectively absorbed at 0.01-5<sup>[4]</sup> of loss tangent. In this study, the porcelain sample did not absorb microwave energy well from 100-600 °C since its loss tangent was low (<0.001), meaning that sample

temperature increased slowly from room temperature until  $\sim 600^\circ\text{C}$ . Above  $600^\circ\text{C}$ , the loss tangent increased exponentially rapidly elevating sample temperature (indicated by the peak  $\sim 600^\circ\text{C}$  in Fig.6b). The second peak at  $800^\circ\text{C}$  in Fig.6b was attributed to strong microwave absorption due to increasing loss tangent resulting from liquid formation from albite melting.

Microwave energy thus produced dense porcelains with promising physical properties at similar temperature compared with the conventional sintering process but microwave substantially reduced processing time. Change of sample loss tangent played an important role in the microwave absorbability and temperature increase. Liquid formation (albite melt) contributed most to the densification of porcelains since it quickly changed the loss tangent. Porcelain samples could be heated from room temperature in a microwave single mode cavity but to produce homogeneous samples insulation and susceptor were required.

In this work, only fully dense CS and MWS samples were used to study the effect of microwaves on microstructural changes (Fig. 7). The low magnification SEI images (Fig. 7a, c) reveal etched microstructures containing mullite, quartz, and glassy phase. CS samples were dense containing mullite and partially dissolved quartz in the glass matrix while MWS samples contained networks of mullite needles grown in the glass matrix. High magnification SEI images (Fig. 7b, d) reveal distinctive mullite morphologies. Mullite crystallite size in CS samples were  $71(\pm 11)$  nm whereas MWS samples were  $56(\pm 9)$  nm (Fig. 8a). CS samples, however, contained low aspect ratio mullite needles ( $\sim 9\pm 2:1$ ) while MWS produced fibre-like mullite with high aspect ratio ( $\sim 32\pm 3:1$ ) (Fig. 8b).

Mullite in porcelains can be differentiated by its aspect ratio. Iqbal and Lee proposed a notation considering the aspect ratio in which type I mullite (primary mullite) exhibits low aspect ratio (1-3:1), type II (secondary mullite) has aspect ratio of 3-10:1, and type III (secondary mullite) possesses very high aspect ratio ( $>30:1$ )<sup>[12]</sup>. Thus, the mullite formed in this porcelain via MWS was type III whilst CS sample was type II.

Mullite crystallite size was also investigated via XRD peak broadening using the Scherer's equation for the (110) plane peak. Calculating the full width half maximum (FWHM) indicated the average mullite crystallite size of CS samples was  $\sim 39(\pm 3)$  nm while MWS sample was  $\sim 28(\pm 3)$  nm. However, mullite crystal sizes

observed from SEM and XRD were different. This may arise from the different sampling volumes of each technique, nonetheless the trends were the same.

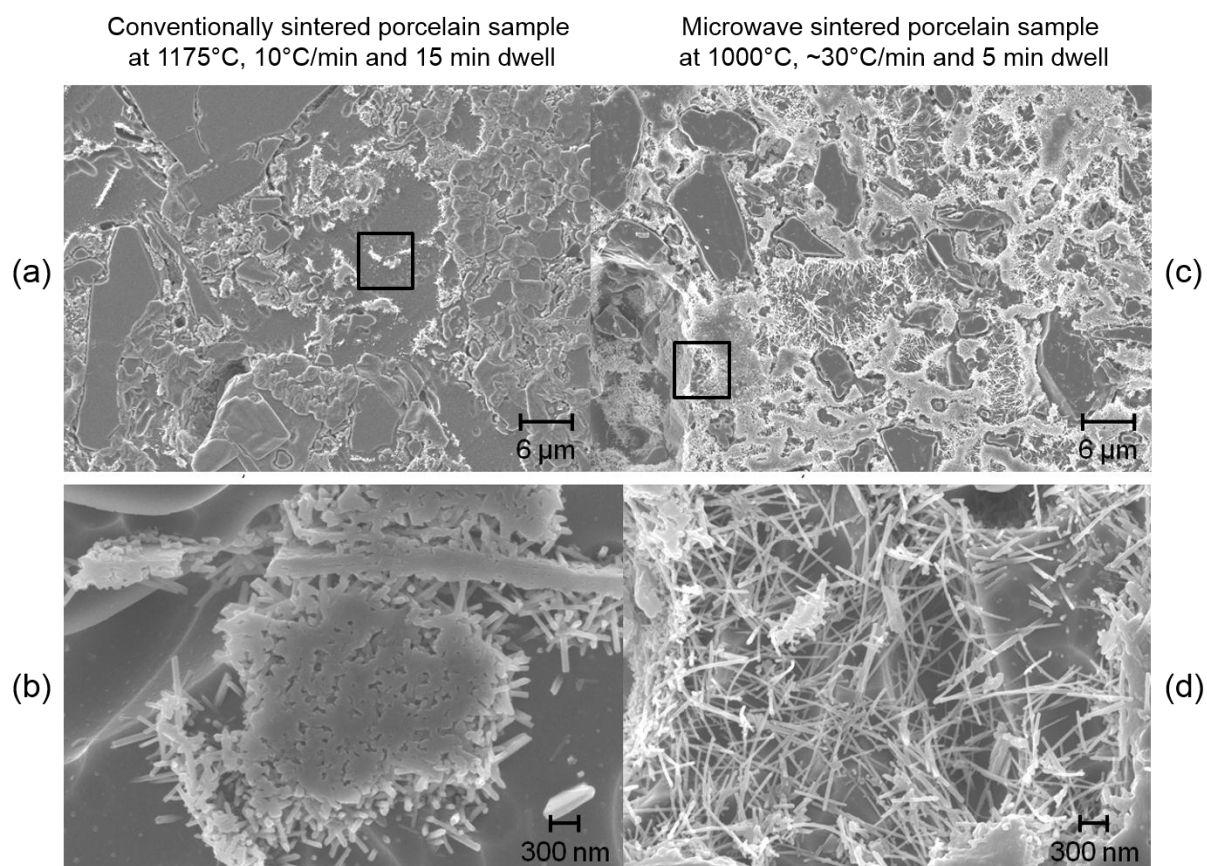


Fig.7. SEM-SEI images of CS and MWS porcelain samples, a) and c) low magnification images showing overall phase content, and b) and d) high magnification images showing the distinctive mullite morphologies.

Mullite usually has acicular morphology with the long fibre axis being the crystal c-axis<sup>[24]</sup>, the c-axis has higher free energy than those in the  $[\text{hk}0]$  directions. Fig. 9a reveals an unusual mullite morphology growing inside a bubble in a MWS sample. Mullite formed in the bubbles was believed to grow via a Vapour-Liquid-Solid (VLS) mechanism<sup>[31, 32]</sup>. Mullite then continually grew in  $[001]$  direction in to the air which had nuclei randomly precipitated on the needles (Fig. 9b-c). These nuclei may assist the growth of high aspect ratio needles. This feature was not observed in CS samples. Also, the formation of mullite via VSL had been not reported in conventional sintering of porcelains.

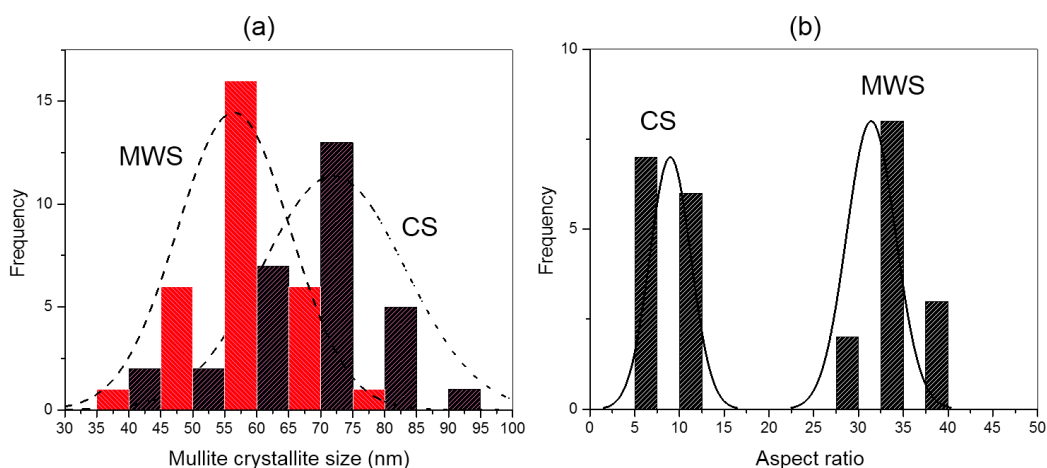


Fig.8. Histograms present (a) crystallite size, and (b) aspect ratio of mullite formed in the porcelain samples under conventional and microwave sintering using SEM analysis.

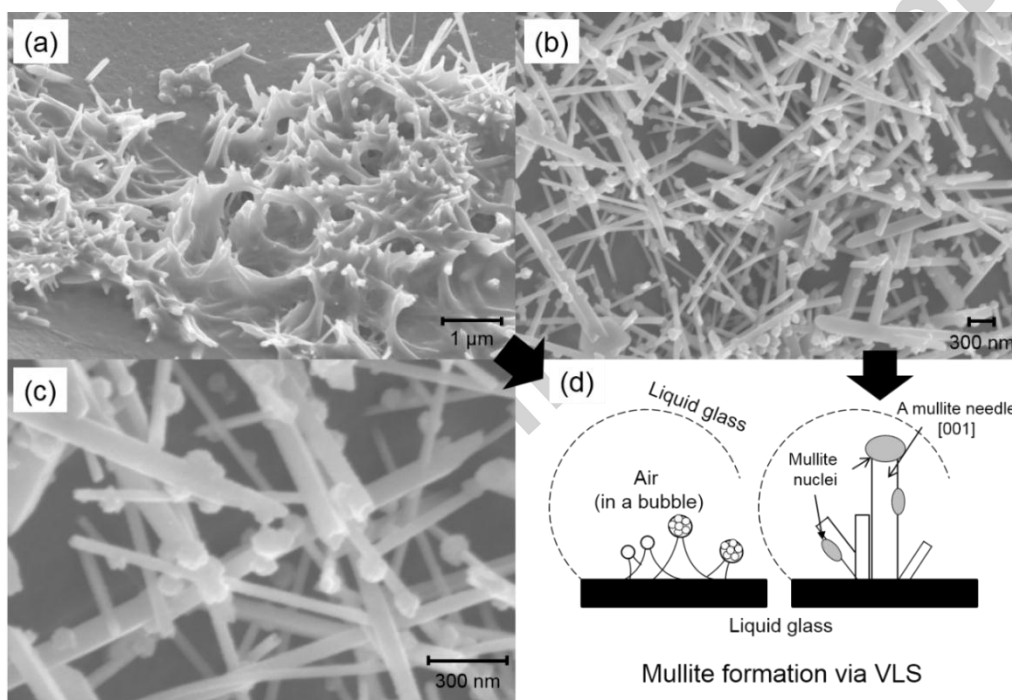


Fig.9. Vapour-Liquid-Solid growth mechanisms of mullite needles under microwave radiation: (a) mullite initially formed in a bubble surrounded by liquid glass phase, (b) mullite needles further grow in bubbles, (c) mullite nuclei precipitated on the mullite needles, and (d) the cartoon diagram showing the growth mechanism.

XRD results (Fig. 10a) reveal MWS samples show larger mullite integrated peak areas suggesting that mullite in this sample formed more than that in the CS samples in agreement with the SEM Image of Fig. 7. CS samples contained smaller peaks of residual albite but not observed in MW samples. It can be deduced that microwave enhanced mullite formation especially from the clays which can be seen

from the microstructures. Number of mullite formed on the clays was more than that form in the glassy phase. In this case, increasing mullite fraction mainly increased from transformation of clays by microwave enhanced reaction rates. It was possible that alumina in albite may be little responsible for mullite formation (in this time range) because there was some of residual albite observed in the MWS sample. A similar result reported that microwave can enhance formation of mullite because a selective heating, and accelerated the nucleation and growth of mullite and changed the mullite formation route of kaolinite [33].

Moreover, the chemical analysis result shows that mullite in MWS samples has more  $Al^{+3}$  than that in CS sample suggesting that mullite should firstly forms via clays decomposition rather than in the liquid glass melt because clays have more molar fraction of alumina compared with the alumina in glass melt. So, it can be conclusive that alumina in albite may be little responsible for mullite formation under microwave radiation in this time scale.

Chemistry of mullite was calculated using the method of Ban and Okada [25] showing molar percent of alumina in mullite. MWS sample mullite had ~63 mol% of alumina compared to ~60 mol% alumina in CS mullite. However, the crystal structures of the mullite in both samples were orthorhombic rather than tetragonal as indicated by the split of (120) and (210) XRD peaks (Fig. 10b and c). The reason why the mullites had different alumina contents may be explained by the effect of the microwave radiation. Formation of MWS mullite was accelerated by reduction of the reaction barriers of  $Al^{+3}$  ions diffusion in the mullite structure [26] which can also be deduced from its fibrous morphology. Moreover, since the liquid glass formed earlier in MWS samples so that the mullite crystals had more time to grow and accommodate alumina into their structures. Thus, MWS mullite had alumina content more than its stoichiometry. Another possibility was the temperature of mullite formation under microwave might be low to obtain the stoichiometric mullite (60 mol%) [27].

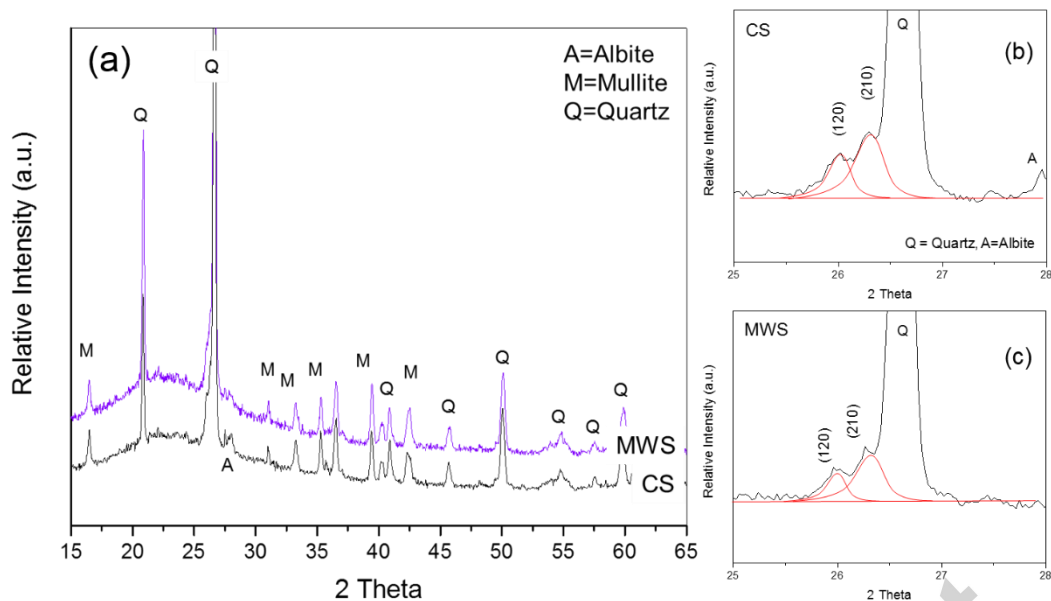


Fig. 10. a) XRD of CS and MWS porcelain samples. Mullite formed under both conditions is identified as orthorhombic mullite by the split of (120) and (210) peaks revealed in b) CS, and c) MWS.

## Conclusions

Porcelain samples were fully sintered using microwave radiation at 1100 °C, a temperature ~75 °C lower than when using a conventional sintering process. Liquid glass phase started to form at ~900-1000°C under microwave radiation while ~1100 °C was required using conventional sintering. Mullite, moreover, formed under microwave radiation had small crystallite size (76 nm) but high aspect ratio (>30:1) compared to mullite from the conventional process. Mullite chemistry in both samples was slightly different; the microwave sintered samples had higher alumina content (~63 mol%) while conventionally sintered samples had stoichiometric mullite (~60 mol%). Both mullites, however, had orthorhombic crystal structure. Formation of mullite was enhanced by microwave energy and may also arise via a vapour-liquid-solid mechanism.

## Acknowledgements

W. Lerdprom acknowledges Imperial College London funding no. MMRE\_PG54200. A. Borrell acknowledges the Spanish Ministry of Economy and Competitiveness for her Juan de la Cierva-Incorporación contract (IJC1-2014-49839).

**References**

1. K.E. Haque, Microwave energy for mineral treatment processes—a brief review, *International Journal of Mineral Processing*, 57(1) (1999)1-24.
2. J.D. Katz, Microwave sintering of ceramics, *Annual Review of Materials Science*, 22(1) (1992) 153-170.
3. D.E. Clark, D.C Folz, What is microwave processing?, in D.E. Clark, D.E. Folz, C.E. Folgar, M.M.Mahmoud (Eds.), *Microwave solutions for ceramics engineers*, The American Ceramic Society, Westerville, Ohio, 2005, pp. 1-32.
4. R.R. Menezes, P.M. Souto, R.H. Kiminami, Microwave fast sintering of ceramic materials, in A. Lakshmanan (Ed.), *Sintering of ceramics-new emerging techniques*, Intech Open Access Publisher, 2012, pp.1-25.
5. V. M. Kenkre, L. Skala, M. W. Weiser, J. D. Katz, Theory of microwave interactions in ceramic materials: the phenomenon of thermal runaway, *Journal of Materials Science*, 26(9) (1991) 2483-2489.
6. J. Wang, J. Binner, B. Vaidhyanathan, N. Joomun, J. Kilner, G. Dimitrakis, T.E. Cross, Evidence for the microwave effect during hybrid sintering, *Journal of the American Ceramic Society*, 89(6) (2006)1977-1984.
7. G. Gaustad, J. Metcalfe, H. Shulman, S. Allan, Susceptor investigation for microwave heating applications, in *Innovative Processing and Synthesis of Ceramics, Glasses and Composites VIII: Proceedings of the 106<sup>th</sup> Annual Meeting of the American Ceramic Society*, Indianapolis, Indiana, 2005, pp. 25-35.
8. H. Shulman, M. Fall, S. Allan. Microwave assist technology for product improvement and energy efficiency. in 4<sup>th</sup> Korea/Japan International Symposium on Material Science and Resources Recycling, Jeju, South Korea, 2007, pp.142-146.
9. D.E. Clark, W.H. Sutton, Microwave processing of materials, *Annual Review of Materials Science*, 26(1) (1996) 299-331.
10. W.E. Webb, R.H. Church, Measurement of dielectric properties of minerals at microwave frequencies, Report of Investigations No. 9035, United State Bureau of Mines, 1986, pp.1-8.
11. W.M. Carty, U. Senapati, Porcelain—Raw materials, processing, phase evolution, and mechanical Behavior. *Journal of the American Ceramic Society*, 81(1) (1998) 3-20.
12. Y. Iqbal, W.E. Lee, Microstructural evolution in triaxial porcelain. *Journal of the American Ceramic Society*, 83(12) (2000) 3121-3127.

13. W. Lerdprom, Firing of porcelain, MS. Thesis, New York State College of Ceramics at Alfred University, Alfred, NY, 2014.
14. Y. Iqbal, W.E. Lee, Fired porcelain microstructures revisited. *Journal of the American Ceramic Society*, 82(12) (1999) 3584-3590.
15. R.R.Menezes, P.M. Souto, R.H. Kiminami, Microwave hybrid fast sintering of porcelain bodies, *Journal of Materials Processing Technology*, 190 (1–3) (2007) 223-229.
16. L.N. Satapathy, Microwave assisted sintering of high voltage porcelain material and its characterization, *Journal of Ceramic Processing Research*, 10(5) (2009) 637-642.
17. S. Allan, M. Fall, H. Shulman, G. Carnahan, Microwave assist sintering of porcelain insulators with large cross section, paper presented at the 33<sup>rd</sup> International Conference and Exposition on Advanced Ceramics and Composites, FL, 2009. Retrieved from <http://www.ceralink.com/sites/default/files/MicrowaveAssistSinteringofPorcelainInsulatorswithLargeCross-section.pdf>
18. T. Santos, L.C. Costa, L. Henrietier, M.A. Valente, J. Monteiro, J. Sousa, Microwave processing of porcelain tableware using a multiple generator configuration, *Applied Thermal Engineering*, 50(1) (2013) 677-682.
19. J. Monteiro, M. A. Valente, T. Santos, L. C. Costa, J. Sousa, Microwave radiation: An alternative method to sinter utilitarian porcelain, in Microwave & Optoelectronics Conference (IMOC), 2011 SBMO/IEEE MTT-S International, Natal, 2011, 561-564.
20. R. Benavente, M.D. Salvador, F.L. Peñaranda-Foix, O. García-Moreno, A. Borrell, High thermal stability of microwave sintered low- $\epsilon_r$   $\beta$ -eucryptite materials, *Ceramics International*, 41(10) (2015) 13817-13822.
21. R. Benavente, A. Borrell, M.D. Salvador, O. Garcia-Moreno, F.L. Peñaranda-Foix, J.M. Catala-Civera, Fabrication of near-zero thermal expansion of fully dense  $\beta$ -eucryptite ceramics by microwave sintering, *Ceramics International*, 40(1) (2014) 935-941.
22. W. Lerdprom, R.K. Chinnam, D.D. Jayaseelan, W.E. Lee, Porcelain production by direct sintering, *Journal of the European Ceramic Society*, 36(16) (2016) 4319-4325.
23. V. Miceli, B. Cioni, A. Lazzeri, Microwave processing of liquid phase sintered alumina, in Proceeding of Materials Science & Technology 2009 Conference and Exhibition, Pittsburgh, PA, 2009, 50-61.
24. P. Hartman, W.G. Perdok, On the relations between structure and morphology of crystals. I. *Acta Crystallographica*, 8(1) (1955) 49-52.

25. T. Ban, K. Okada, Structure refinement of mullite by the Rietveld method and a new method for estimation of chemical composition, *Journal of the American Ceramic Society*, 75(1) (1992) 227-230.
26. M. Panneerselvam, K.J. Rao, Novel microwave method for the synthesis and sintering of mullite from kaolinite, *Chemistry of Materials*, 15(11) (2003) 2247-2252.
27. C.G. Bergeron, S. H. Risbud. Introduction to phase equilibria in ceramics, Wiley-American Ceramic Society, Ohio, USA, 1986.
28. B.R. Johnson, W.M. Kriven, J. Schneider, Crystal structure development during devitrification of quenched mullite, *Journal of European Ceramics Society*, 21(14) (2001), 2541-2562.
29. B. Sonupalak, M. Sarakaya, I.A. Aksay, Spinel phase formation during the 980°C exothermic reaction in the kaolinite-to-mullite reaction series, *Journal of American Ceramic Society*, 70(11) (1987), 837-842.
30. W. Lerdprom, C.Li, D.D Jayaseelan, S. J. Skinner, W.E. Lee, Temperature dependence of electrical conductivity of a green porcelain mixture, *Journal of the European Ceramic Society*, 37(1) (2017) 343-349.
31. C. Cerecedo, V. Valcárcel, M. Gómez, I. Drubi, F. Guitián, New massive vapor-liquid-solid deposition of  $\alpha$ -Al<sub>2</sub>O<sub>3</sub> fibers, *Advance Engineering Materials*, 9(7) (2007) 600–603.
32. L. Dan, Y. Xiumin, C. Jian, J. Fang, Y. Yong, H. Zhengren, L. Xuejian, Microstructure and reaction mechanism of SiC ceramic with mullite-zircon as a new liquid-phase sintering additives system, *Materials Science and Engineering: A*, 559, (2013) 510-514.
33. Z. Zhang, X. Qiao, J. Yu, Microwave selective heating-enhanced reaction rates for mullite preparation from kaolinite, *RSC Advances*, 4(6) (2014) 2640-2647.